Design of a Linear Model Predictive Controller for an Overactuated Triangular Floating Platform

Aristomenis Tsopelakos, *Student Member, IEEE*, Kostas Vlachos, and
Evangelos Papadopoulos, *Senior Member, IEEE*

***Abstract*— In this paper the design of a linear model predictive controller for a triangular floating platform is presented aiming at the stabilization of its linear and angular velocities as well as its position and orientation. Three rotating jets, located at the corners of the platform, control its motion. With this control configuration, the platform is over-actuated. The prediction, and optimization phase of the linear model predictive controller are presented in detail. Simulation results, in the presence of realistic environmental disturbances, are given that demonstrate the performance and robustness of the controller. The proposed controller is compared with a model-based controller that was developed for the same platform in a prior work, and the superiority of the former concerning the dynamic positioning capabilities, and the power consumption is shown.**

I. Introduction

Floating platforms are widely used in the petroleum industry, as portable pipeline systems, as research, in-the-field laboratories, etc. [1]. To accomplish their tasks, these platforms must be kept stationary at a desired position and orientation. Therefore, they are equipped with appropriate actuation systems that provide the necessary dynamic positioning forces to counter balance the sea wave, wind and current induced forces and moments, and all uncertainties [2]. Floating platform dynamics are inherently nonlinear due to the strong hydrodynamic interactions [3].

Model predictive controllers for marine vehicles have been proposed in the past but mostly for the heading and the tracking control of ships [4-5]. A model predictive controller is presented in [6] for an autonomous underwater vehicle. A nonlinear model predictive control scheme for the track keeping of inland vessels is presented in [7]. Typically, floating platforms have redundant actuation, i.e., they are over-actuated system. Hence, control allocation schemes that distribute the closed-loop control forces and moments efficiently have been developed [8-9].

In this paper, the authors present the design of a model predictive controller, aiming at the dynamic positioning of the overactuated triangular floating platform Vereniki, see insert of Fig. 1. Three rotating jets control the triangular platform, one on each of its corners. The system is overactuated, hence, an appropriate control allocation scheme is employed to allow for optimal allocation of the effort without violating thruster capabilities. The scheme aims at stabilizing the platform position and orientation under actuator constraints, and in the presence of realistic environmental disturbances.

The authors presented early results on marine platform dynamic positioning in [10], where a model-based controller and a proper control allocation scheme were proposed. In this work, a linear model predictive controller is proposed, which minimizes an optimization cost function that includes the states errors, and the control effort, showing considerably better positioning results. Moreover, according to simulation results, the developed linear model predictive controller is robust, and shows less power consumption, with respect to the previously developed model-based controller. Simulation results, including environmental disturbances such as sea currents, wind generated waves, and wind forces validate the performance of the controller.

II. A Brief Description of the Platform "Vereniki"

"Vereniki" is designed to assist in the deployment of the deep-sea cubic kilometer neutrino telescope "NESTOR" (www.nestor.noa.gr). It consists of a triangular structure mounted on three hollow double-cylinders, one at each corner of the structure, see Fig. 1.

The plane of the triangle is parallel to the sea surface. The cylinders provide the necessary buoyancy, as part of them is immersed in the water. The actuation is realized using three fully submerged pump-jets, located at the bottom of each cylinder. Diesel engines drive the pumps, while electro-hydraulic motors rotate the jets providing vectored thrust.

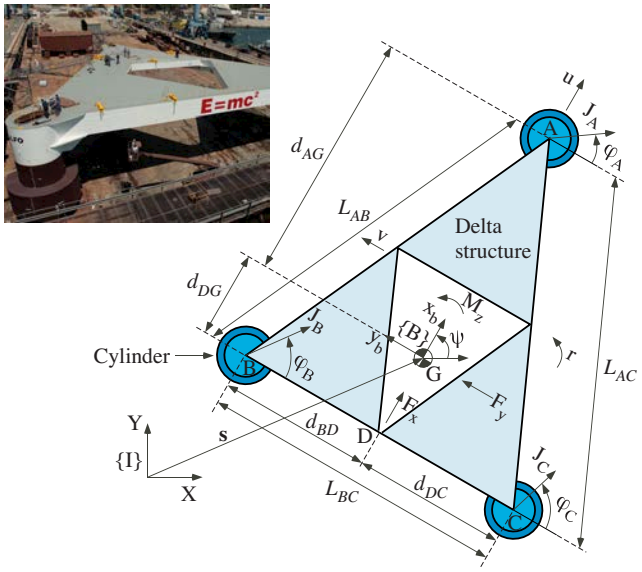

Figure 1. The platform Vereniki, and its 2D graphical representation.

A. Tsopelakos is with the Department of Electrical and Computer Engineering, National Technical University of Athens, 15780 Athens, Greece, (e-mail: tsopelakosaris121@yahoo.gr).

K. Vlachos, and E. Papadopoulos are with the Department of Mechanical Engineering, National Technical University of Athens, 15780 Athens, Greece, (e-mail: {kostaswl; egpapado}@central.ntua.gr).

A. Kinematics

The main body of the structure has the shape of an isosceles triangle with side length $L_{AB} = L_{AC}$, and base length L_{BC}. The center of mass (CM) of the platform is at point G, see Fig. 1.

We focus on the platform planar motion; actuation and control along the heave axis, and about the roll and pitch axes, are beyond the scope of this work. Under these assumptions, the kinematics equations of the plane motion are described by:

$$\begin{bmatrix} \dot{x} \\ \dot{y} \\ \dot{\psi} \end{bmatrix} = \begin{bmatrix} \mathrm{c}\psi & -\mathrm{s}\psi & 0 \\ \mathrm{s}\psi & \mathrm{c}\psi & 0 \\ 0 & 0 & 1 \end{bmatrix} \begin{bmatrix} u \\ v \\ r \end{bmatrix} \Rightarrow {}^{I}\dot{\mathbf{x}} = {}^{I}\mathbf{J}_{B}\,{}^{B}\mathbf{v} \quad (1)$$

with s· = sin(·), and c· = cos(·). In (1), x and y represent the platform CM inertial coordinates and ψ describes the orientation of the body-fixed frame {B}, whose origin is at the platform CM; u and v are the surge and sway velocities respectively, defined in the body-fixed frame {B}, and r is the yaw (angular) velocity of the platform.

B. Dynamics

We consider three types of forces acting on the CM of the platform: (a) the control forces/ torque from the jets, (b) the hydrodynamic forces due to the motion of the cylinders with respect to the water, and (c) the environmental disturbance forces/ torque due to wind, sea current, and waves.

1) Control forces/ torque

The jets can provide vectored thrust and thus more flexibility in control design. The J_A, J_B, and J_C in Fig. 1 denote the magnitudes of the thrusts while φ_A, φ_B, and φ_C denote the force directions. These thrusts provide control resultant forces in x_b and y_b axes, the $F_{c,x}$ and $F_{c,y}$ respectively acting on the CM, and a torque $N_{c,z}$ about z_b, according to the linear transformation:

$${}^{B}\boldsymbol{\tau}_c = [F_{c,x}, F_{c,y}, N_{c,z}]^T = \mathbf{B}\,{}^{B}\mathbf{f}_c \quad (2a)$$

$$\mathbf{B} = \begin{bmatrix} 1 & 0 & 0 \\ 0 & -1 & -d_{AG} \\ 1 & 0 & -d_{DC} \\ 0 & -1 & d_{DG} \\ 1 & 0 & d_{DC} \\ 0 & -1 & d_{DG} \end{bmatrix}^T, \quad {}^{B}\mathbf{f}_c = \begin{bmatrix} J_A s\varphi_A \\ J_A c\varphi_A \\ J_B s\varphi_B \\ J_B c\varphi_B \\ J_C s\varphi_C \\ J_C c\varphi_C \end{bmatrix} \quad (2b)$$

where ${}^{B}\boldsymbol{\tau}_c$ is the control force/ torque vector, and the dimensional parameters in $\mathbf{B}$ are defined in Fig. 1. The vector ${}^{B}\mathbf{f}_c$ can be retrieved by the pseudoinversion of $\mathbf{B}$ in (2a). The desired jet thrust and direction are calculated according to,

$$J_i = \sqrt{(f_i \mathrm{s}\varphi_i)^2 + (f_i \mathrm{c}\varphi_i)^2}, \quad \varphi_i = a\tan 2(f_i \mathrm{s}\varphi_i, f_i \mathrm{c}\varphi_i) \quad (3)$$

where $i = A, B, C$.

2) Hydrodynamic forces

The hydrodynamic force acting on each cylinder includes two terms. The first term is the added mass force, which is a linear function of the acceleration of each cylinder. The second term is the drag force, which is a quadratic function of the velocity of each cylinder, see [11-12]. As an example, the normal to the axis of each cylinder force on the double-cylinder structure at point A, expressed in body-fixed frame {B} is given by:

$$\begin{aligned} {}^{B}\mathbf{f}_{h,A} = {} & C_a \pi \rho_w [R_{uc}^2 (H_{uc} - h) + R_{lc}^2 H_{lc}]({}^{B}\dot{\mathbf{v}}_{wat}^{\perp} - {}^{B}\mathbf{a}_A) \\ & + C_d \rho_w [R_{uc}(H_{uc} - h) + R_{lc} H_{lc}] \left\| ({}^{B}\mathbf{v}_{wat}^{\perp} - {}^{B}\mathbf{v}_A) \right\| \\ & \cdot ({}^{B}\mathbf{v}_{wat}^{\perp} - {}^{B}\mathbf{v}_A) \end{aligned} \quad (4)$$

where ρ_w is the water density, C_a is the added mass coefficient, and C_d the drag coefficient. ${}^{B}\mathbf{v}_A$ and ${}^{B}\mathbf{a}_A$ are the velocity and acceleration of cylinder A respectively. ${}^{B}\mathbf{v}_{wat}^{\perp}$ is the component of the velocity vector of the water normal to the axis of each cylinder, calculated from the vectorial addition of the sea current velocity, and the water flow velocity due to sea waves, all expressed in the body-fixed frame. Parameters h, R_{uc}, H_{uc}, R_{lc}, and H_{lc} denote the height of the cylinder above the water surface, and the radius and height of the upper and lower cylinder sections respectively.

The hydrodynamic forces on A given by (4) result in a force acting on the platform CM and a moment about it, i.e.,

$${}^{B}\mathbf{q}_{h,A} = \left[{}^{B}\mathbf{f}^{T}{}_{h,A},\ ({}^{B}\mathbf{s}_{A/G} \times {}^{B}\mathbf{f}_{h,A})^T \right]^T \quad (5)$$

where ${}^{B}\mathbf{s}_{A/G}$ is the position of point A with respect to G expressed in {B}, see Fig. 1. All terms that are a quadratic function of the velocity of the platform are collected in vector

$${}^{B}\mathbf{q} = [f_x, f_y, n_z]^T \quad (6)$$

3) Environmental disturbances

We define the disturbance vector ${}^{B}\mathbf{q}_{dist}$, which represents wind and wave generated disturbance forces and torques. Integrating Gaussian white noise produces the inertial sea current and wind velocity magnitude and direction used in the simulations. The inertial sea current velocity magnitude, $v_c(t)$, is limited such that $v_c(t) \le 0.514$ m/s (1 kn). The wind velocity magnitude, $v_w(t)$, is limited such that $v_w(t) \le 7.9$ m/s (15 kn or 4 Beaufort). The maximum values for the disturbances are defined after analyzing weather and marine data, collected at the NESTOR site. The models used for the simulation of the forces/ torque due to wind, and waves can be found in [13].

Using the above preliminaries, and assuming that the CM of the platform is at the triangle's centroid, we derive the planar equations of motion of the platform, in {B}:

$$\mathbf{M}\,{}^{B}\dot{\mathbf{v}} = {}^{B}\mathbf{q} + {}^{B}\mathbf{q}_{dist} + {}^{B}\boldsymbol{\tau}_c \quad (7a)$$

$$\mathbf{M} = \begin{bmatrix} m - 3m_a & 0 & 0 \\ 0 & m - 3m_a & 0 \\ 0 & 0 & m_{33} \end{bmatrix} \quad (7b)$$

$$m_{33} = I_{zz} - (d_{AG}^2 + 2d_{BD}^2 + 2d_{DG}^2)m_a$$

where m is the mass of the platform, m_a is its added mass, and I_{zz} is its mass moment of inertia about the z_b axis.

4) Actuators dynamics

The control force/ torque vector ${}^{B}\boldsymbol{\tau}_c$ is due to the rotating jets. However, the desired jet thrust and direction cannot be applied immediately because of actuator dynamics and limitations. The jet thrust, and rotation dynamics are modeled as first order lags:

$$\dot{J}_i = (1/\tau_J)(J_{i,des} - J_i)$$
$$\dot{\varphi}_i = (1/\tau_\varphi)(\varphi_{i,des} - \varphi_i) \quad (8)$$

where τ_φ, and τ_J are the jet thrust, and rotation time constant. The actuator limitations include the jet rotation speed limit, and the maximum thrust limit. A more comprehensive description of the kinematics and dynamics of the platform can be found in [10].

III. Design of the Linear Model Predictive Controller

The design is divided into two distinct steps. The first is the linearization of the model of the platform and the second is the application of the linear model predictive control algorithm [14].

1) Step 1

Starting from (7a), it holds that,

$$^B\boldsymbol{\tau}_c = \mathbf{M}\,{}^B\dot{\mathbf{v}} - {}^B\mathbf{q} - {}^B\mathbf{q}_{dist} \quad (9)$$

Using (1) and its derivative, $^B\dot{\mathbf{v}}$ is written as,

$$^B\dot{\mathbf{v}} = {}^I\mathbf{J}_B^{-1}({}^I\ddot{\mathbf{x}} - {}^I\dot{\mathbf{J}}_B\,{}^B\mathbf{v}) \quad (10)$$

and combining (9) and (10), the open-loop dynamics of the platform is described by

$$^B\boldsymbol{\tau}_c = \mathbf{M}\,{}^I\mathbf{J}_B^{-1}\,{}^I\ddot{\mathbf{x}} - \mathbf{M}\,{}^I\mathbf{J}_B^{-1}\,{}^I\dot{\mathbf{J}}_B\,{}^I\mathbf{J}_B^{-1}\,{}^I\dot{\mathbf{x}} - {}^B\mathbf{q} - {}^B\mathbf{q}_{dist} \quad (11)$$

Setting the control vector equal to

$$^B\boldsymbol{\tau}_c = \mathbf{M}\,{}^I\mathbf{J}_B^{-1}\mathbf{f}_{fb} - \mathbf{M}\,{}^I\mathbf{J}_B^{-1}\,{}^I\dot{\mathbf{J}}_B\,{}^I\mathbf{J}_B^{-1}\,{}^I\dot{\mathbf{x}} - {}^B\mathbf{q} \quad (12)$$

where $\mathbf{f}_{fb}$ is an auxiliary control input, the system closed-loop dynamics is written as,

$$\ddot{\mathbf{x}} = \mathbf{f}_{fb} - {}^I\mathbf{J}_B\mathbf{M}^{-1}\,{}^B\mathbf{q}_{dist} \quad (13)$$

which is a double integrator with the following state space equations:

$$\dot{\mathbf{x}}_s = \begin{bmatrix} \mathbf{0}_{3\times3} & \mathbf{I}_{3\times3} \\ \mathbf{0}_{3\times3} & \mathbf{0}_{3\times3} \end{bmatrix}\mathbf{x}_s + \begin{bmatrix} \mathbf{0}_{3\times3} \\ \mathbf{I}_{3\times3} \end{bmatrix}\mathbf{f}_{fb}$$
$$\mathbf{y} = \begin{bmatrix} \mathbf{I}_{3\times3} & \mathbf{0}_{3\times3} \end{bmatrix}\mathbf{x}_s \quad (14a)$$

with

$$\mathbf{x}_s = [x, y, \psi, \dot{x}, \dot{y}, \dot{\psi}]^T \quad (14b)$$

The matrices $\mathbf{I}_{n\times n}$ and $\mathbf{0}_{n\times n}$ denote the n×n identity, and zero matrix respectively. The vector $^I\mathbf{J}_B\mathbf{M}^{-1\,B}\mathbf{q}_{dist}$ is considered as external bounded disturbance.

2) Step 2

In this step, we design the auxiliary control input, $\mathbf{f}_{fb}$, applying a linear model predictive control scheme. $\mathbf{f}_{fb}$ stabilizes the plant and in the same time minimizes the following cost function:

$$J = \int_0^{T_p} (\mathbf{x}_{aug}(t_i + \tau \mid t_i)^T \mathbf{Q}\mathbf{x}_{aug}(t_i + \tau \mid t_i) + \dot{\mathbf{f}}_{fb}{}^T\mathbf{R}\dot{\mathbf{f}}_{fb})\,dt \quad (15)$$

where $\mathbf{x}_{aug}(t_i+\tau|t_i)$ is the prediction of the state vector of an augmented model, described next, in the time interval $[t_i, t_i+T_p]$. $\mathbf{Q}$ and $\mathbf{R}$ are weighting matrices, and T_p is the prediction horizon. These are design parameters.

As we can see in (15), the cost function includes the derivative of the auxiliary control input, $\mathbf{f}_{fb}$. In order to compute the derivative of the control we create an augmented model with a state vector, $\mathbf{x}_{aug}$, that includes the derivative of the state vector of the double integrator (14), augmented by the observed variables x, y, ψ, i.e.

$$\mathbf{x}_{aug} = [\dot{x}, \dot{y}, \dot{\psi}, \ddot{x}, \ddot{y}, \ddot{\psi}, x, y, \psi]^T \quad (16)$$

The augmented model is described by the following state space equations:

$$\dot{\mathbf{x}}_{aug} = \begin{bmatrix} \mathbf{0}_{3\times3} & \mathbf{I}_{3\times3} & \mathbf{0}_{3\times3} \\ \mathbf{0}_{3\times3} & \mathbf{0}_{3\times3} & \mathbf{0}_{3\times3} \\ \mathbf{I}_{3\times3} & \mathbf{0}_{3\times3} & \mathbf{0}_{3\times3} \end{bmatrix}\mathbf{x}_{aug} + \begin{bmatrix} \mathbf{0}_{3\times3} \\ \mathbf{I}_{3\times3} \\ \mathbf{0}_{3\times3} \end{bmatrix}\dot{\mathbf{f}}_{fb}$$
$$= \mathbf{A}\mathbf{x}_{aug} + \mathbf{B}\dot{\mathbf{f}}_{fb}$$
$$\mathbf{y}_{aug} = \begin{bmatrix} \mathbf{0}_{3\times6} & \mathbf{I}_{3\times3} \end{bmatrix}\mathbf{x}_{aug} \quad (17)$$

and the derivative of the control is computed as a state feedback, i.e.

$$\dot{\mathbf{f}}_{fb} = -\mathbf{K}_{mpc}\mathbf{x}_{aug}(t) \quad (18)$$

Our goal is to determine the matrix $\mathbf{K}_{mpc}$. This will be achieved from the predictive control analysis. After the computation of the optimal trajectory of the derivative of $\mathbf{f}_{fb}$, we integrate it, and we feed the plant with only the initial value. Then we compute again the optimal trajectory having as initial state the new state of the plant.

The derivative of the control input is approximated by a set of orthonormal functions, i.e.

$$\dot{\mathbf{f}}_{fb}(t) \approx \begin{bmatrix} \mathbf{L}_1(t)^T\boldsymbol{\eta}_1 \\ \mathbf{L}_2(t)^T\boldsymbol{\eta}_2 \\ \mathbf{L}_3(t)^T\boldsymbol{\eta}_3 \end{bmatrix} \quad (19a)$$

with

$$\mathbf{L}_j = [l_1, ..., l_{N_j}],\quad \boldsymbol{\eta}_j = [c_1, ..., c_{N_j}],\quad j = 1,2,3 \quad (19b)$$

where j is equal the size of the auxiliary control input vector, $\mathbf{f}_{fb}$, and $l_i(t)$, $i = 1, 2, \ldots, N_j$, are the Laguerre orthonormal functions used for the approximation, which are defined as

$$l_i(t) = \sqrt{2}p\frac{e^{pt}}{(i-1)!}\frac{d^{i-1}}{dt}[t^{i-1}e^{-2pt}] \quad (20)$$

p is the time scaling factor for the Laguerre functions, which determines their exponential decay rate, and is a design parameter. The accuracy of the approximation in (19a) increases as the number of the Laguerre orthonormal functions, N_j, increases. N_j is also a design parameter. By solving (17) in time, we compute the future prediction of $\mathbf{x}_{aug}(t)$ for $t_i \le \tau \le t_i + T_p$, i.e.

$$\mathbf{x}(t_i + \tau \mid t_i) = e^{\mathbf{A}\tau}\mathbf{x}(t_i) + \boldsymbol{\varphi}(\tau)^T\boldsymbol{\eta} \quad (21a)$$

where

$$\boldsymbol{\varphi}(\tau)^T = \int_0^\tau e^{\mathbf{A}(\tau-\gamma)}[\mathbf{B}_1\mathbf{L}_1(\gamma)^T, ..., \mathbf{B}_j\mathbf{L}_j(\gamma)^T]\,d\gamma \quad (21b)$$

The matrix $\boldsymbol{\varphi}(\tau)^T$ is expressed as

$$\boldsymbol{\varphi}(\tau)^{\mathrm{T}} = [\boldsymbol{\varphi}_1(\tau)^T, \boldsymbol{\varphi}_2(\tau)^T, \boldsymbol{\varphi}_3(\tau)^T] \quad (22)$$

where the dimension of $\boldsymbol{\varphi}_i(\tau)$ is equal to $n \times N_i$, i = 1, 2, 3 and n is the dimension of $\mathbf{x}_{aug}$. The matrix $\boldsymbol{\varphi}_i(\tau)^T$ is the solution of the following linear algebraic equation:

$$\mathbf{A}\boldsymbol{\varphi}_i(\tau)^T - \boldsymbol{\varphi}_i(\tau)^T \mathbf{A}_{p_i}^T = -\mathbf{B}_i \mathbf{L}_i(\tau)^T + e^{\mathbf{A}\tau}\mathbf{B}_i \mathbf{L}_i(0)^T \quad (23a)$$

where

$$\mathbf{A}_{p_i} = \begin{bmatrix} -p & 0 & \cdots & 0 \\ -2p & -p & \cdots & 0 \\ \vdots & \vdots & \ddots & \vdots \\ -2p & \cdots & -2p & -p \end{bmatrix} \quad (23b)$$

and the dimension of $\mathbf{A}_{pi}$ is $N_i \times N_i$.

The optimal coefficient matrix $\boldsymbol{\eta} = [\boldsymbol{\eta}_1, \boldsymbol{\eta}_2, \boldsymbol{\eta}_3]^T$ that minimizes (15) for $t_i \le \tau \le t_i + T_p$, is given by

$$\boldsymbol{\eta} = -\boldsymbol{\Omega}^{-1}\boldsymbol{\Psi}\mathbf{x}_{aug}(t_i) \quad (24)$$

where

$$\boldsymbol{\Omega} = \int_0^{T_p} \boldsymbol{\varphi}(\tau)\mathbf{Q}\boldsymbol{\varphi}(\tau)^T d\tau + \mathbf{R}_L, \quad \boldsymbol{\Psi} = \int_0^{T_p} \boldsymbol{\varphi}(\tau)\mathbf{Q}e^{\mathbf{A}\tau} d\tau \quad (25)$$

Assuming that $\mathbf{R}$ is a diagonal matrix with $\mathbf{R} = diag\{r_1, r_2, r_3\}$, the $\mathbf{R}_L$ is a block diagonal matrix with the j-th block being $\mathbf{R}_j = r_j \mathbf{I}_{Nj \times Nj}$, where N_j is the number of Laguerre functions used to approximate the derivative of the j-th input.

Hence, the whole trajectory, in the prediction horizon, of the derivative of the control input can be constructed as

$$\dot{\mathbf{f}}_{fb}(\tau) = \begin{bmatrix} \mathbf{L}_1(\tau)^T & 0 & 0 \\ 0 & \mathbf{L}_2(\tau)^T & 0 \\ 0 & 0 & \mathbf{L}_3(\tau)^T \end{bmatrix} \begin{bmatrix} \boldsymbol{\eta}_1 \\ \boldsymbol{\eta}_2 \\ \boldsymbol{\eta}_3 \end{bmatrix} \quad (26)$$

According to the receding horizon control principle, in each cycle of computation we keep only the initial value of the whole trajectory, so the state feedback law is given by (18) with

$$\mathbf{K}_{mpc} = \begin{bmatrix} \mathbf{L}_1(0)^T & 0 & 0 \\ 0 & \mathbf{L}_2(0)^T & 0 \\ 0 & 0 & \mathbf{L}_3(0)^T \end{bmatrix} \boldsymbol{\Omega}^{-1}\boldsymbol{\Psi} \quad (27)$$

IV. Simulation Results

In this section, we are presenting a simulation example of the developed linear model predictive controller. Our goal is to stabilize the floating platform position in a circle with center (0,0) and a radius equal to 5 m and the platform direction at 0 deg., with a tolerance equal to ±5 deg.

The position and orientation of the real platform are supplied from GPS receivers mounted at the platform vertices. For the simulation runs, sensor noise (±1 m), acquired from the real GPS readings, is added to the position and orientation data. The simulation is held with environmental disturbances, such as wind, see Fig. 2 (a, c, and e), and wave forces, see Fig. 2 (b and d). The wind velocity is depicted in Fig. 2f. The platform must overcome the environmental disturbances without exceeding the jet thrust limit, which is 20 kN for each one, and the jet rotation velocity limit which is 0.84 rad/s, for each one. The simulation time is 600 s.

The initial position is set as x = 20.0 m, y = 20.0 m, ψ = -20.0 deg, u = 0.1 m/s, v = -0.1 m/s, r = -0.01 rad/s. Some characteristic parameters are given: d_{AG} = 26.694 m, d_{BD} = 18.241 m, R_{uc} = 2.2 m, H_{uc} = 6.3 m, R_{lc} = 3.4 m, H_{lc} = 3.0 m and the hydrodynamic coefficients are C_a = 0.55, C_d = 0.8. The sea water density is ρ = 1025 kg/m^3, the mass of the platform is $m = 425\times10^3$ kg. The design parameters of the controller are chosen as shown in Table I. The resulting trajectory of the center mass of the platform in the inertial 2D space is displayed in Fig. 3.

TABLE I. Design Parameters of the Controller

Parameter	p_1, p_2, p_3	N_1, N_2, N_3	T_p	**Q**	**R**
Value	2, 2, 1	2, 2, 2	400 s	$\mathbf{I}_{9\times9}$	$10^8\times\mathbf{I}_{3\times3}$

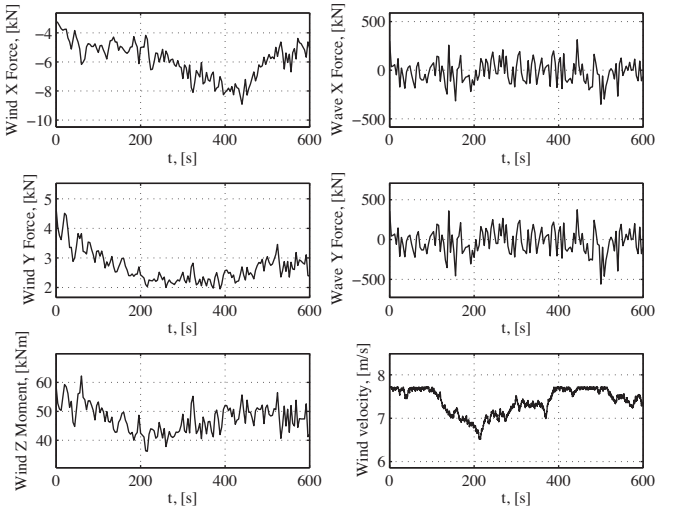

Figure 2. Environmental disturbances for the simulation run.

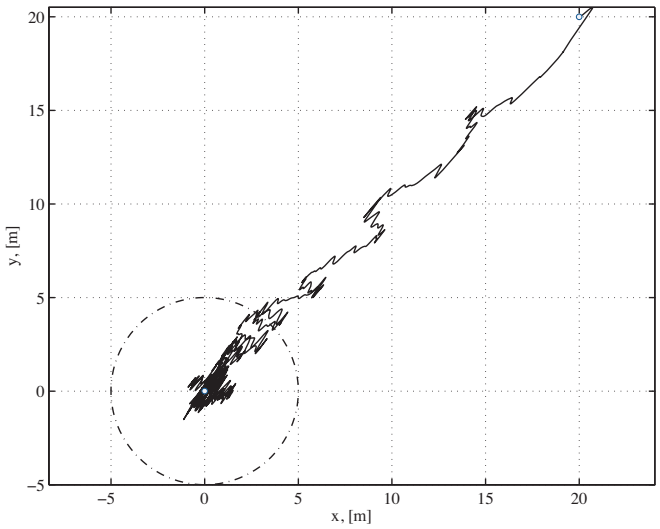

Figure 3. The 2D path of the CM of the platform.

The platform position and orientation is depicted in Fig. 4 (a, c, and e), while Fig. 4 (b, d, and f) shows the linear and angular velocities. As shown in Fig. 3 and 4, the platform is stabilized within the required limits, despite the disturbances and actuators constraints.

Fig. 5 shows the thrusts of the jets and the corresponding angles. The jet rotation, and thrust time constants are $\tau_\varphi = 1$ s and $\tau_J = 3$ s. Note that the jet thrusts and angles are relatively smooth. In addition, the resulted forces and torque acting on the CM of the platform are shown in Fig. 6.

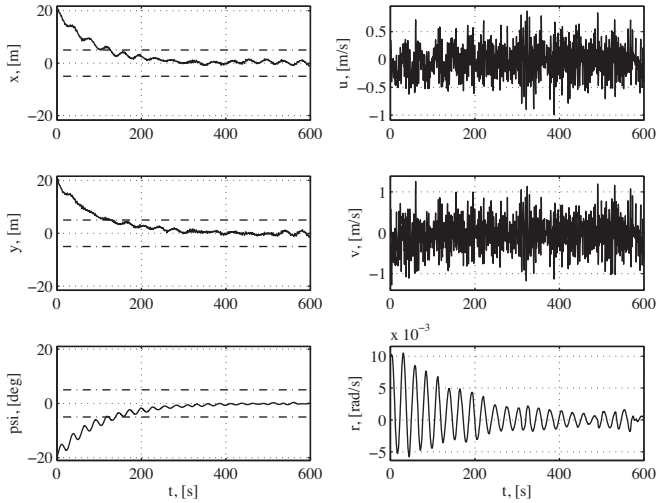

Figure 4. (a), (c), (e) Position and orientation, and (b), (d), (f) Velocities.

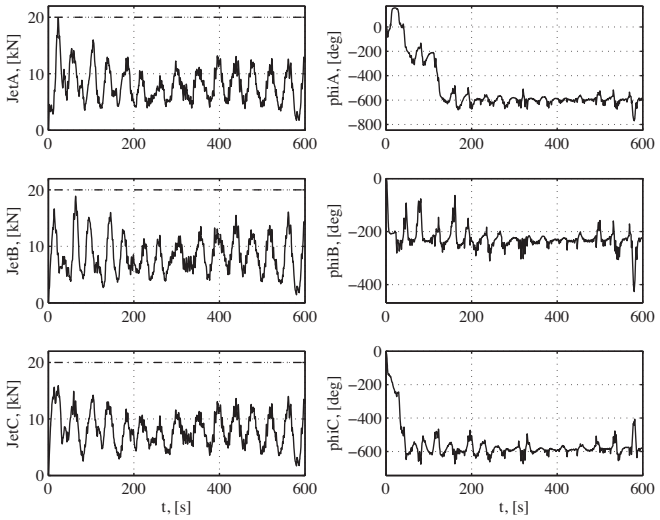

Figure 5. (a), (c), (e) Jet thrusts, and (b), (d), (f) Jet angles.

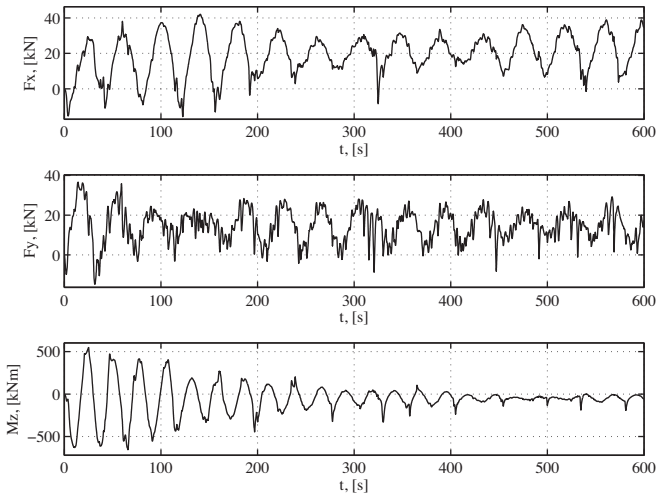

Figure 6. Resulted forces and torque acting on the CM of the platform.

Discussion on the robustness of the controller

The first step on the design of the linear MPC is the linearization of the model of the platform by setting the control vector equal to (12). In order to evaluate the robustness of the controller against uncertainties in the parameters of (12), we executed four simulation runs, varying the estimated mass of the platform. During the simulation runs, the average jet energy consumption of the three jets, and the integral of the squared error inside the circle of radius 5m were calculated. The results are shown in Table II.

TABLE II. EXAMINATION OF ROBUSTNESS

Estimated mass error (%)	-50	-60	-90	-95
Integral of the squared error ($m^2 \times sec$)	677.88	715	785.7	860
Average energy consumption (kJ)	44.44	44.19	45.33	47.15

The results indicate that even for a difference of -95% between the estimated and the true value of the platform's mass, the controller manages to stabilize it within the required limits. Moreover, there is no significant variation in the average energy consumption.

Comparison to a model-based controller

The responses of the linear model predictive controller and the model-based controller, presented in [10], are compared next. The gains of the model-based controller were chosen as $k_{dx} = k_{dy} = k_{d\psi} = 0.105$, $k_{px} = k_{py} = k_{p\psi} = 0.0037$, and $k_{ix} = k_{iy} = k_{i\psi} = 0.000043$. The simulation runs were executed under the same environmental disturbances, actuator constraints, and measurement noise. Fig. 7 displays the positioning results.

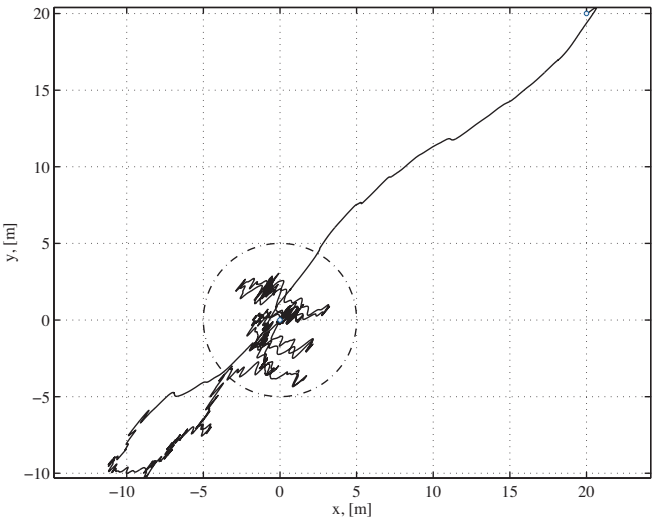

Figure 7. The 2D path of the CM of the platform with the model-based controller from [10].

In this figure, one can observe that, although the platform is stabilized within the required limits, the linear model predictive controller results in a much better response. The resulting platform CM path, depicted in Fig. 3 and Fig. 7, shows that the linear model predictive controller achieves an average position error reduction of about 15% of that of the model-based controller.

The platform position and orientation trajectories, using the model-based controller, are depicted in Fig. 8 (a, c, and e), while Fig. 8 (b, d, and f) shows the linear and angular

velocities. In addition, Fig. 9 shows the thrusts of the jets and the corresponding angles, while the resulted forces and torque acting on the CM of the platform are shown in Fig. 10.

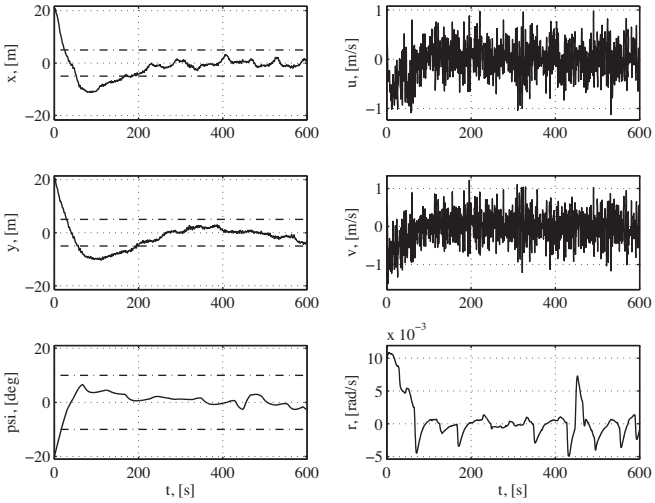

Figure 8. (a), (c), (e) Position and orientation, and (b), (d), (f) Velocities, with the model-based controller from [10].

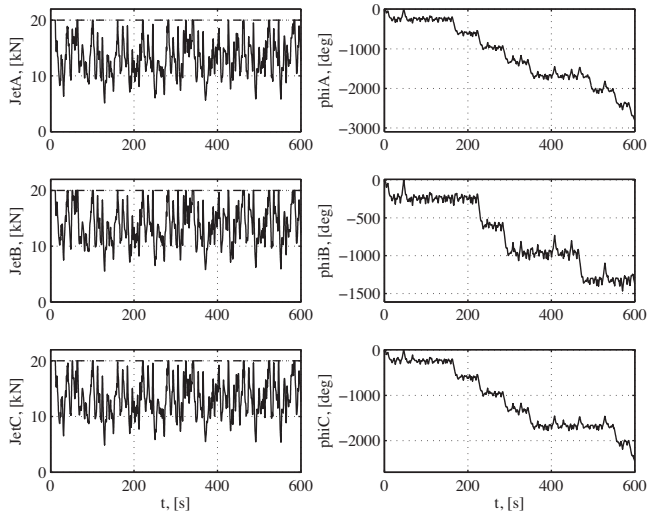

Figure 9. (a), (c), (e) Jet thrusts, and (b), (d), (f) Jet angles, with the model-based controller from [10].

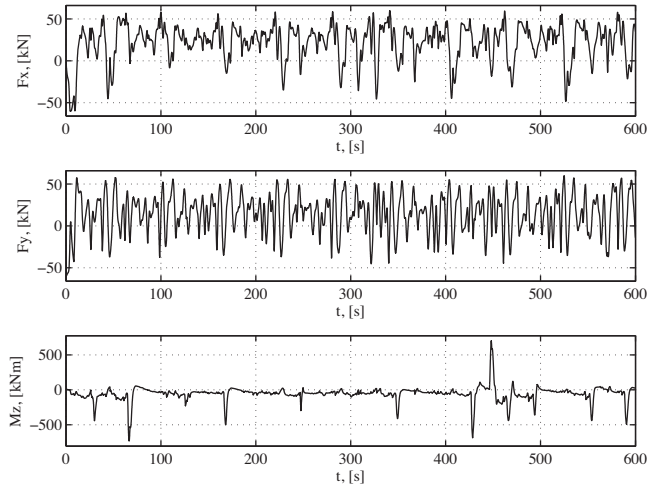

Figure 10. Resulted forces and torque acting on the CM of the platform, with the model-based controller from [10].

Based on the thrusts of the jets shown in Fig. 5 and Fig. 9, we calculated that there is a reduction in the average energy consumption of the three jets of about 43%.

V. Conclusion

We presented the design of a linear model predictive controller aiming at the dynamic positioning of an overactuated triangular floating platform. The system is over-actuated, i.e., it has more control inputs than DOF. Hence, an appropriate control allocation scheme was developed in order to realize the control objective without violating thruster capabilities. Simulation results illustrated its performance, under realistic actuator constraints, and hardware limitations including thrust upper limit and delay. The developed controller is validated under wind, and wind generated wave environmental disturbances. A comparison, under the same conditions and constraints, is performed between the linear model predictive controller presented here, and a model-based controller that was developed for the same platform in a previous work. The comparison indicates the superiority of the former concerning its dynamic positioning capabilities, and the power consumption. Simulation results showed that using the linear model predictive controller, a reduction in the average energy consumption, and in the position error of about 43%, and 15% respectively is achieved.

References

[1] Wilson, J. F., *Dynamics of Offshore Structures*, New Jersey, John Wiley and Sons, 2003.

[2] Sørensen, A. J., "A Survey of Dynamic Positioning Control Systems," in *Annual Reviews in Control*, vol. 35, no. 1, pp. 123-136, April 2011.

[3] Hawary, F. E. (Ed.), *The Ocean Engineering Handbook*. Boca Raton, Florida, CRC Press, 2001.

[4] Zhen L. and Sun, J., "Disturbance Compensating Model Predictive Control with Application to Ship Heading Control," *IEEE Transactions on Control Systems Technology*, vol. 20, no.1, Jan. 2012, pp. 257-265.

[5] Ghaemi, R., Soryeok Oh, and Sun, J., "Path following of a model ship using Model Predictive Control with experimental verification," *American Control Conference (ACC), 2010*, June 30-July 2, 2010, pp. 5236-5241.

[6] Medagoda, L. and Williams, S.B., "Model predictive control of an autonomous underwater vehicle in an in situ estimated water current profile," *OCEANS, 2012 - Yeosu*, 21-24 May 2012, pp.1-8.

[7] Wahl, A. and Gilles, E., "Track-keeping on waterways using model predictive control," in *Proc. IFAC Conf. Control Applications Marine Systems*, 1998, pp. 149–154.

[8] Johansen, T. A. and Fossen, T. I. "Control allocation—a survey," *Automatica*, 49(5), 2013, pp. 1087-1103.

[9] Vermillion, C., Sun, J., and Butts, K., "Model predictive control allocation for overactuated systems - stability and performance," *46th IEEE Conference on Decision and Control, 2007*, 12-14 Dec. 2007, pp.1251-1256.

[10] Vlachos, K. and Papadopoulos, E., "Control design and allocation of an over-actuated triangular floating platform," *2010 IEEE International Conference on Robotics and Automation (ICRA)*, 3-7 May 2010, pp. 3739-3744.

[11] Hoerner, S. F., *Fluid-Dynamic Drag*, Hoerner Publications, 1965.

[12] "Recommended Practice for Planning, Designing and Constructing Fixed Offshore Platforms-Working Stress Design," *American Petroleum Institute (API)*, 21st edition, December 2000.

[13] Fossen, T. I., *Guidance and Control of Ocean Vehicles*, John Wiley & Sons, 1994.

[14] Wang, Liuping, *Model Predictive Control System Design and Implementation Using MATLAB®*, in Advances in Industrial Control, Series Editors: M.J. Grimble and M.A. Johnson, Springer-Verlag, 2009.